Journal of Quantitative Spectroscopy & Radiative Transfer 110 (2009) 1640–1653

Contents lists available at ScienceDirect

Journal of Quantitative Spectroscopy & Radiative Transfer

journal homepage: www.elsevier.com/locate/jqsrt

Test of Mie-based single-scattering properties of non-spherical dust aerosols in radiative flux calculations

Q. Fu [a,b,*], T.J. Thorsen [a], J. Su [a,b], J.M. Ge [a,b], J.P. Huang [b]

[a] Department of Atmospheric Sciences, University of Washington, Seattle, WA 98195, USA
[b] College of Atmospheric Sciences, Lanzhou University, Lanzhou 730000, PR China

ARTICLE INFO

Article history:
Received 30 December 2008
Received in revised form
6 March 2009
Accepted 10 March 2009

Keywords:
Dust aerosols
Non-spherical particles
Optical properties
Mie
Radiative fluxes

ABSTRACT

We simulate the single-scattering properties (SSPs) of dust aerosols with both spheroidal and spherical shapes at a wavelength of 0.55 μm for two refractive indices and four effective radii. Herein spheres are defined by preserving both projected area and volume of a non-spherical particle. It is shown that the relative errors of the spheres to approximate the spheroids are less than 1% in the extinction efficiency and single-scattering albedo, and less than 2% in the asymmetry factor. It is found that the scattering phase function of spheres agrees with spheroids better than the Henyey–Greenstein (HG) function for the scattering angle range of 0–90°. In the range of ~90–180°, the HG function is systematically smaller than the spheroidal scattering phase function while the spherical scattering phase function is smaller from ~90° to 145° but larger from ~145° to 180°.

We examine the errors in reflectivity and absorptivity due to the use of SSPs of equivalent spheres and HG functions for dust aerosols. The reference calculation is based on the delta-DISORT-256-stream scheme using the SSPs of the spheroids. It is found that the errors are mainly caused by the use of the HG function instead of the SSPs for spheres. By examining the errors associated with the delta-four- and delta-two-stream schemes using various approximate SSPs of dust aerosols, we find that the errors related to the HG function dominate in the delta-four-stream results, while the errors related to the radiative transfer scheme dominate in the delta-two-stream calculations. We show that the relative errors in the global reflectivity due to the use of sphere SSPs are always less than 5%. We conclude that Mie-based SSPs of non-spherical dust aerosols are well suited in radiative flux calculations.

1. Introduction

Dust aerosol, which is the dominant aerosol by mass in the climate system [1], scatters and absorbs solar radiation, and absorbs and emits longwave radiation, leading to significant tropospheric heating but surface cooling [2,3]. Dust aerosol also influences the regional and global climate through its indirect effects by serving as cloud condensation nuclei [4,5] and delivering iron nutrient to oceans [6]. Dust aerosol occurs naturally but is exacerbated in many instances by human impacts on land use and soil moisture [7].

* Corresponding author at: Department of Atmospheric Sciences, University of Washington, Seattle, WA 98195, USA. Tel.: +1 206 685 2070; fax: +1 206 543 0308.
E-mail address: qfu@atmos.washington.edu (Q. Fu).

0022-4073/$ - see front matter © 2009 Elsevier Ltd. All rights reserved.
doi:10.1016/j.jqsrt.2009.03.010

The shapes of dust aerosols are exclusively non-spherical [8–10]. It is well recognized that the scattering phase functions of non-spherical dust aerosols are vastly different from those of equivalent spheres based on Mie theory [9,11,12]. It is thus critically important to take into account the non-spherical effect when retrieving dust aerosol optical and microphysical properties from the measurements of solar radiances [11–15].

However, it is a common practice to use Mie theory to approximate the single-scattering properties (SSPs) of dust aerosols in the radiative flux calculations [16–19]. Mishchenko et al. [11] showed that the spherical and non-spherical differences in the extinction coefficient, single-scattering albedo, and asymmetry factor for dust aerosols become smaller than those in the scattering phase function so that the influence of the particle shapes on the aerosol radiative forcing is small. But so far there is no systematic assessment of the application of equivalent spheres to dust aerosols in the solar radiative flux calculations.

This paper will address the following questions. First, what are the errors in the solar radiative fluxes associated with solar reflectivity and absorptivity of a dust layer by using the extinction coefficient, single-scattering albdeo, and scattering phase function from Mie theory? To address this question we will represent a single non-spherical particle by a collection of monodisperse spheres which contains the same total surface area and total volume as the original particle [20]. The SSPs of such defined spheres can represent those of non-spherical particles better than using spheres with either equivalent projected area or equivalent volume [20–23]. Second, how accurate is the Henyey–Greenstein (HG) function to represent the scattering phase function of dust aerosols in the radiative flux calculations? The HG scattering phase function that is based on a single parameter, the asymmetry factor, is exclusively used in the radiative flux calculations in the climate models. This practice greatly simplifies the parameterization of dust aerosol SSPs. And third, how do errors related to the use of equivalent spheres and the HG function compare to errors due to the delta-two- and delta-four-stream radiative transfer schemes that are widely used in climate models?

In Section 2 of this paper we describe the SSPs of dust aerosols used in this study. Section 3 describes the radiative flux calculations and how the above questions are addressed. Results and conclusions are presented in Sections 4 and 5, respectively.

2. Single-scattering properties

The SSPs of non-spherical dust aerosols are calculated following Yang et al. [12]. The shapes of dust particles are assumed to be spheroids [11,15] with an aspect ratio (i.e., a/b where a and b are the rotational-symmetry and equatorial semi-axes, respectively) of 1.7 [24]. 1000 size bins are considered with a (b) ranging from 0.071 (0.042) to 21.37 (12.57) μm with a resolution $\Delta \ln a$ of 0.0057. The refractive indices of dust particles compiled by Levoni et al. [18] are used, which show little spectral dependence of the imaginary (real) part for wavelengths $<\sim 2$ (1) μm. (Note that this may not be true for imaginary part of the dust refractive index at short wavelengths where spectral dependence can be significant [25].) The refractive index is $1.53+0.008i$ at the wavelength of 0.55 μm. For a sensitivity test, we also consider a refractive index of $1.53+0.001i$ for dust particles with much weaker absorption.

To compute the SSPs of spheroidal dust particles, a combination of the T-matrix method [26] and an approximate method is used. The T-matrix method is applied to spheroids with a size parameter smaller than 50. Here the size parameter is defined as $2\pi r_v/\lambda$ where λ is the wavelength and r_v is the radius of the equivalent sphere with the same volume as a spheroid (see more discussions below). The approximate method, which is applied to spheroids with a size parameter larger than 50, employs the improved geometric optics method (IGOM) [27] to compute the scattering phase function. In the calculation of extinction and absorption efficiencies, the contribution of the so-called edge effects is added to the IGOM results [12]. The spheroids are assumed to be randomly oriented in space. The SSPs including the extinction and absorption efficiencies and scattering phase functions from the T-matrix and the approximate methods converge well at a size parameter of $\sim$40 to 50 [12].

The volume (V) of a spheroid is given by $V = 4/3\pi ab^2$. The surface area (S) for a prolate spheroid (i.e., $a/b \geqslant 1.0$) is given by $S = 2\pi b^2 + 2\pi ab \sin^{-1}\varepsilon/\varepsilon$ where ε is the eccentricity of the spheroid and $\varepsilon = \sqrt{a^2 - b^2}/a$. The projected area ($P$) of a randomly oriented convex particle is $S/4$ [28]. To apply Mie theory, non-spherical particles are usually converted into spheres using either an equivalent projected area or an equivalent volume [10,11]. The radius for a projected area equivalent sphere is $r_p = (P/\pi)^{1/2}$ while the radius for a volume equivalent sphere is $r_v = (3V/4\pi)^{1/3}$. Note that under the geometric optics limit, the extinction and absorption cross sections are largely determined by P and V [23]. By using a sphere with r_p, the extinction cross section of a non-spherical particle is exact but the absorption cross section is overestimated. By using a sphere with r_v, the extinction cross section is underestimated.

For a non-spherical particle, spheres with a radius r_{vp} can also be defined with both equivalent projected area and volume. By letting $P = \pi r_{vp}^2 n$ and $V = (4/3)\pi r_{vp}^3 n$, where n is an adjusted number of spheres to preserve both P and V for a non-spherical particle, we have $r_{vp} = 3V/4P$. Note that n here does not have to be an integer. By using n spheres with r_{vp}, both extinction and absorption cross sections of a non-spherical particle are well represented under geometric optics limit. Note that the ratio of volume to projected area (V/P) of a non-spherical particle is conserved in the sphere with r_{vp}, which is a fundamental parameter in determining the absorption efficiency of the particle [29,30]. The advantage of using equal-V/P spheres over the equal-area spheres or equal-volume spheres has been documented in many literatures [20–23,31,32]. In this study, we apply Mie calculation to spheres with r_{vp} to mimic the SSPs of non-spherical dust aerosols.

The radiative impact of dust aerosols depends strongly on their size distribution. Here we represent the dust aerosol size distribution in terms of r_v, consistent with the ground-based remote sensing algorithms that retrieve the particle volume distribution [15,33]. The lognormal distribution following Levoni et al. [18] is employed in this study

$$\frac{dN(r_v)}{dr_v} = \frac{N_0}{r_v\ \ln(10)\sigma\sqrt{2\pi}} \exp\left\{-\frac{[\log(r_v/r_{vm})]^2}{2\sigma^2}\right\}, \tag{2.1}$$

where r_{vm} and σ are the mode radius and standard deviation, respectively; N_0 is the number density of dust aerosols; and σ is set to be 0.4. This size distribution is the same as the standard model of the accumulation mode of dust aerosol adopted in the Multiangle Imaging SpectroRadiometer (MISR) aerosol retrieval algorithm [11,34] but using the volume-equivalent spheres. In this study the r_v ranges from 0.05 to 15 μm, corresponding to a (b) from 0.071 (0.042) to 21.37 (12.57) μm, with a resolution $\Delta \ln r_v$ of 0.0057. Note that for a given aspect ratio of a spheroid, among the four measures of its sizes, i.e., $a(b)$, r_{vp}, r_v, and r_p, we can determine uniquely the other three from a given one (e.g., r_v).

The radiative impact of size distributions of spherical particles can be largely represented by an effective radius as defined by Hansen and Travis [35]. For non-spherical dust aerosols, we can define the effective radius (r_e) using the V/P-equivalent spheres [22] in the form

$$r_e = \frac{\int_{r_{v,\min}}^{r_{v,\max}} r_{vp}^3 nN(r_v)\,dr_v}{\int_{r_{v,\min}}^{r_{v,\max}} r_{vp}^2 nN(r_v)\,dr_v} = \frac{3}{4}\frac{\int_{r_{v,\min}}^{r_{v,\max}} VN(r_v)\,dr_v}{\int_{r_{v,\min}}^{r_{v,\max}} PN(r_v)\,dr_v}, \tag{2.2}$$

where for a given r_v, n is the number of spheres with a radius r_{vp} corresponding to a spheroid that has a volume V and a projected area P.

For a given size distribution, the bulk SSPs of the dust aerosols including the mean extinction efficiency (Q_e), single-scattering albedo ($\tilde{\omega}$), and scattering phase function (P_{11}) can be written as follows:

$$Q_e = \frac{\int_{r_{v,\min}}^{r_{v,\max}} Q_e' PN(r_v)\,dr_v}{\int_{r_{v,\min}}^{r_{v,\max}} PN(r_v)\,dr_v}, \tag{2.3a}$$

$$\tilde{\omega} = \frac{\int_{r_{v,\min}}^{r_{v,\max}} Q_s' PN(r_v)\,dr_v}{\int_{r_{v,\min}}^{r_{v,\max}} Q_e' PN(r_v)\,dr_v}, \tag{2.3b}$$

$$P_{11} = \frac{\int_{r_{v,\min}}^{r_{v,\max}} P_{11}' Q_s' PN(r_v)\,dr_v}{\int_{r_{v,\min}}^{r_{v,\max}} Q_s' PN(r_v)\,dr_v}, \tag{2.3c}$$

where Q_e', Q_s' and P_{11}' are the extinction and scattering efficiencies and the scattering phase function, respectively, for an individual particle. For a given r_v, the SSPs including Q_e', Q_s' and P_{11}' are computed from a combination of the T-matrix and the approximate methods for the spheroid, and from Mie theory for the V/P-equivalent sphere. It is noted that all the SSPs are a function of the wavelength in general.

3. Radiative flux calculations

We consider a dust layer with various optical depths and incident solar zenith angles. We use effective radii of 0.25, 0.5, 1.0, and 2.0 μm for the dust aerosol size distributions. The discrete-ordinates (DISORT) method [36] with the delta-adjustment [37] is employed in the radiative flux calculations. The bulk scattering phase function is expanded in terms of Legendre polynomials P_l in the form

$$P_{11}(\cos\theta) = \sum_{l=0}^{N} \tilde{\omega}_l P_l(\cos\theta), \tag{3.1a}$$

where θ is the scattering angle and the moment $\tilde{\omega}_l$ can be determined from the orthogonal properties of Legendre polynomials in the form

$$\tilde{\omega}_l = \frac{2l+1}{2}\int_{-1}^{1} P_{11}(\cos\theta)P_l(\cos\theta)\,d\cos\theta. \tag{3.1b}$$

In our notations, $\tilde{\omega}_0 = 1$ and $\tilde{\omega}_1/3 = g$, the asymmetry factor. Herein we expand the scattering phase function into 256 terms (i.e., $N = 255$) and perform the δ-256-stream calculations.

The SSPs of non-spherical dust aerosols are used in the reference calculations. We examine the errors due to the use of SSPs of V/P-equivalent spheres. The errors due to the HG function in representing the scattering phase function are also examined. The HG function is defined in the form

$$P_{HG}(\cos\theta) = \frac{1-g^2}{(1+g^2-2g\cos\theta)^{3/2}}. \tag{3.2}$$

Table 1
Single-scattering properties (SSPs) of dust aerosols including extinction efficiency (Q_e), single-scattering albedo ($\tilde{\omega}$), and asymmetry factor (g) at the wavelength of 0.55 μm with the refractive indices of 1.53+0.008*i* and 1.53+0.001*i* for both spheroids and *V*/*P*-equivalent spheres with the effective radii of 0.25, 0.5, 1.0, and 2.0 μm.

r_e (μm)	m = 1.53+0.008*i*			m = 1.53+0.001*i*		
	Q_e	$\tilde{\omega}$	g	Q_e	$\tilde{\omega}$	g
Spheroid						
0.25	1.8037	0.9435	0.6763	1.8048	0.9921	0.6639
0.50	2.4225	0.9201	0.7022	2.4312	0.9877	0.6790
1.00	2.5630	0.8742	0.7272	2.5706	0.9778	0.6882
2.00	2.4069	0.7995	0.7731	2.4093	0.9574	0.7118
Sphere						
0.25	1.8093 (0.3)	0.9440 (0.1)	0.6656 (−1.6)	1.8102 (0.3)	0.9922 (0.0)	0.6555 (−1.3)
0.50	2.4409 (0.8)	0.9216 (0.2)	0.6924 (−1.4)	2.4495 (0.8)	0.9881 (0.0)	0.6747 (−0.6)
1.00	2.5814 (0.7)	0.8775 (0.4)	0.7208 (−0.9)	2.5890 (0.7)	0.9791 (0.1)	0.6928 (0.7)
2.00	2.4197 (0.5)	0.8048 (0.7)	0.7710 (−0.3)	2.4227 (0.6)	0.9608 (0.4)	0.7279 (2.3)

The numbers in parentheses are the relative errors in the SSPs using the *V*/*P*-equivalent spheres to approximate the spheroids.

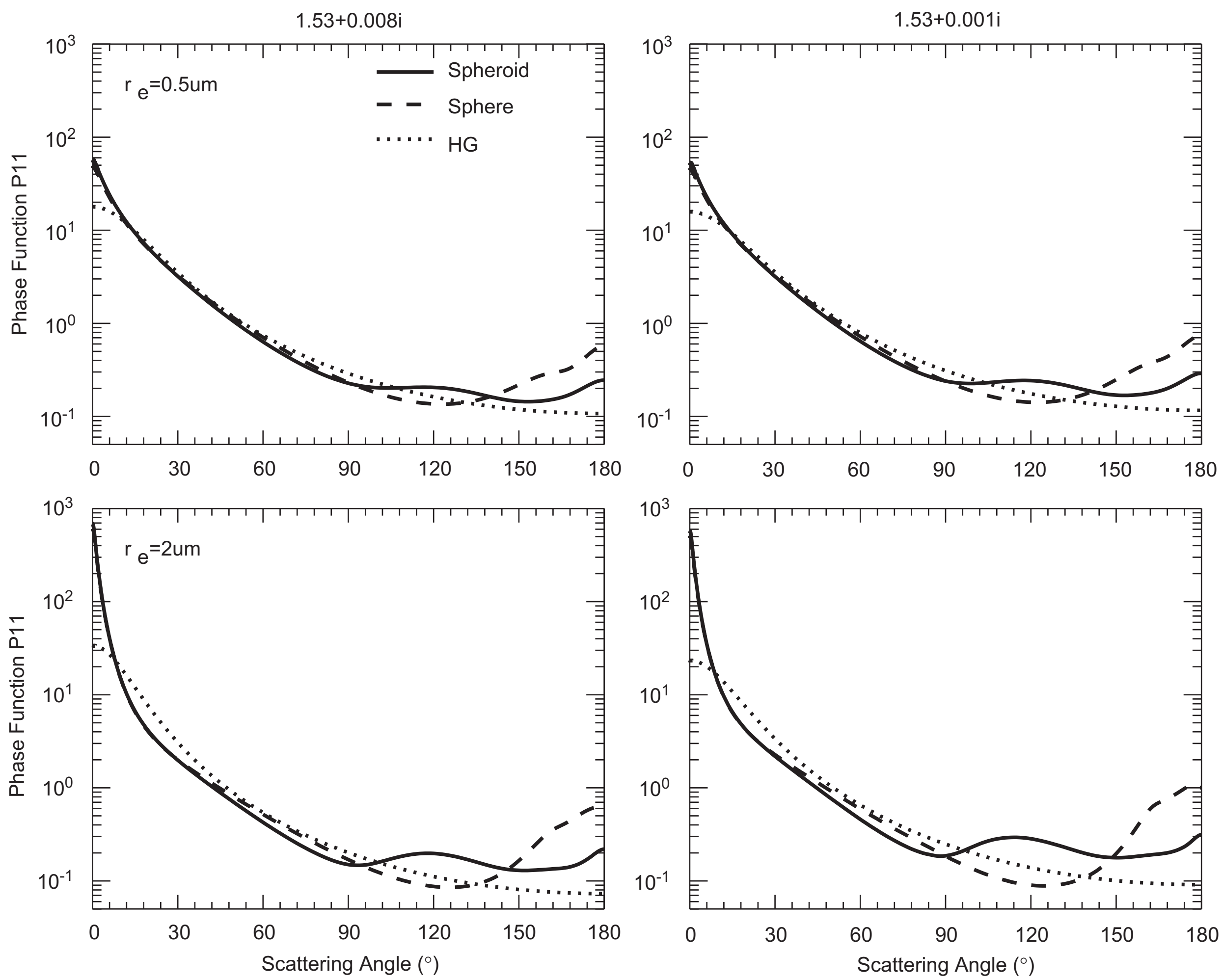

Fig. 1. Dust aerosol scattering phase functions based on spheroids (solid line), *V*/*P*-equivalent spheres (dashed line), and Henyey–Greenstein (HG) function using the asymmetry factor of spheroids (dotted line), at the wavelength of 0.55 μm for the refractive indices of 1.53+0.008*i* (left panel) and 1.53+0.001*i* (right panel) and the effective radii of 0.5 μm (upper panel) and 2 μm (lower panel).

Note that $\tilde{\omega}_l = (2l+1)g^l$ for the HG function. Furthermore the errors of these approximations in representing dust aerosol SSPs are compared to errors due to the radiative transfer parameterizations such as the delta-two- and delta-four-stream approximations [38]. These approximations are commonly used in the global climate models.

We examine and compare the errors related to various approximations in the solar reflectivity and absorptivity at the wavelength of 0.55 μm. For a dust layer with an optical depth τ_1, the optical depth at the top and bottom of the layer is zero and τ_1, respectively. The reflectivity r and absorptivity a are then defined in the forms

$$r(\mu_0) = F^{\uparrow}(0)/\mu_0 F_0, \tag{3.3a}$$

$$a(\mu_0) = [\mu_0 F_0 - F^{\uparrow}(0) + F^{\uparrow}(\tau_1) - F^{\downarrow}(\tau_1)]/\mu_0 F_0, \tag{3.3b}$$

where μ_0 is the cosine of the solar zenith angle, F_0 is the incident solar flux perpendicular to the solar beam, and $F^{\uparrow}$ and $F^{\downarrow}$ are the upward and downward fluxes, respectively. We use a surface albedo of zero in our calculations so that r is the reflectivity of the dust layer only. We also examine the global albedo that is defined in the form

$$\bar{r} = 2\int_0^1 r(\mu_0)\mu_0\, d\mu_0. \tag{3.4}$$

Under the single-scattering limit when τ_1 is very small, the solar reflectivity can be expressed analytically, which is useful to check and interpret the errors as derived from numerical experiments. Under this limit, the bidirectional reflectance R for the direct incident solar radiation at the direction $(-\mu_0,\phi_0)$ that is reflected to the direction (μ,ϕ) is [39]

$$R(-\mu_0, \phi_0; \mu, \phi) = \tau_1 \frac{\tilde{\omega}}{4\mu\mu_0} P_{11}(-\mu_0, \phi_0; \mu, \phi). \tag{3.5}$$

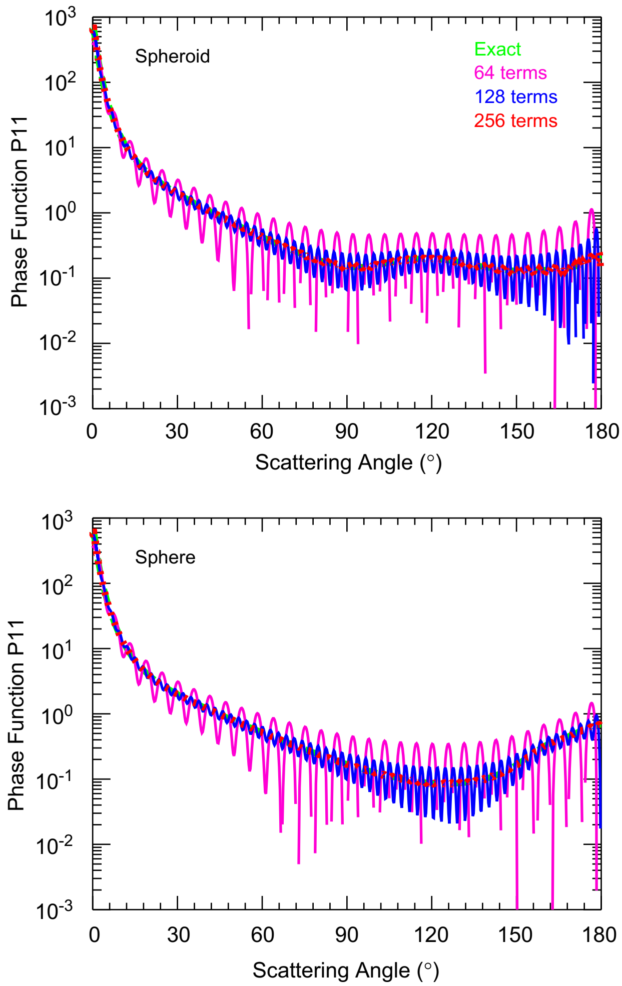

Fig. 2. Dust aerosol scattering phase functions based on spheroids (upper panel) and V/P-equivalent spheres (lower panel) at the wavelength of 0.55 μm for the refractive index of 1.53+0.008i and the effective radius of 2 μm, and their expansions in terms of Legendre polynomials with 64, 128, and 256 terms.

The solar reflectivity is related to the bidirectional reflectance by

$$r(\mu_0) = \frac{1}{\pi}\int_0^{2\pi}\int_0^1 R(-\mu_0, \phi_0; \mu, \phi)\mu\, d\mu\, d\phi. \tag{3.6}$$

Insert Eq. (3.5) into Eq. (3.6) and note that $1/2\pi\int_0^{2\pi} P_{11}(\cos\theta)\, d\phi = \sum_{l=0}^{N}\tilde{\omega}_l P_l(\mu)P_l(\mu')$. Also note that $\int_0^1 P_l(\mu)\, d\mu = (-1)^{(l-1)/2}((l-2)!!/(l+1)!!)$ when l is an odd number, but one when $l=0$, and zero when l is an even number. We have

$$r(\mu_0) = \frac{\tau_1\tilde{\omega}}{2\mu_0}\left[1 + \sum_{i=0}^{(N-1)/2} a_i\tilde{\omega}_{2i+1}P_{2i+1}(-\mu_0)\right], \tag{3.7}$$

where $a_i = (-1)^i(2i-1)!!/(2i+2)!!$. In Section 4, we will also present the errors in $r(\mu_0)$ due to the use of the approximate SSPs under the single-scattering limit following Eq. (3.7).

4. Numerical results and discussions

4.1. Single-scattering properties

Table 1 shows the SSPs of dust aerosols with both spheroidal and V/P-equivalent-spherical shapes at a wavelength of 0.55 μm for two refractive indices and four effective radii. The SSPs are very sensitive to the effective radius of dust aerosols. For example, for the refractive index of 1.53+0.008i, when r_e increases from 0.25 to 2 μm, $\tilde{\omega}$ decreases from 0.9435 to 0.7995 while g increases from 0.6763 to 0.7731. Both single-scattering albedo and asymmetry factor also depend on the imaginary part (m_i) of refractive indices. Table 1 shows that the relative errors due to the use of the V/P-equivalent spheres

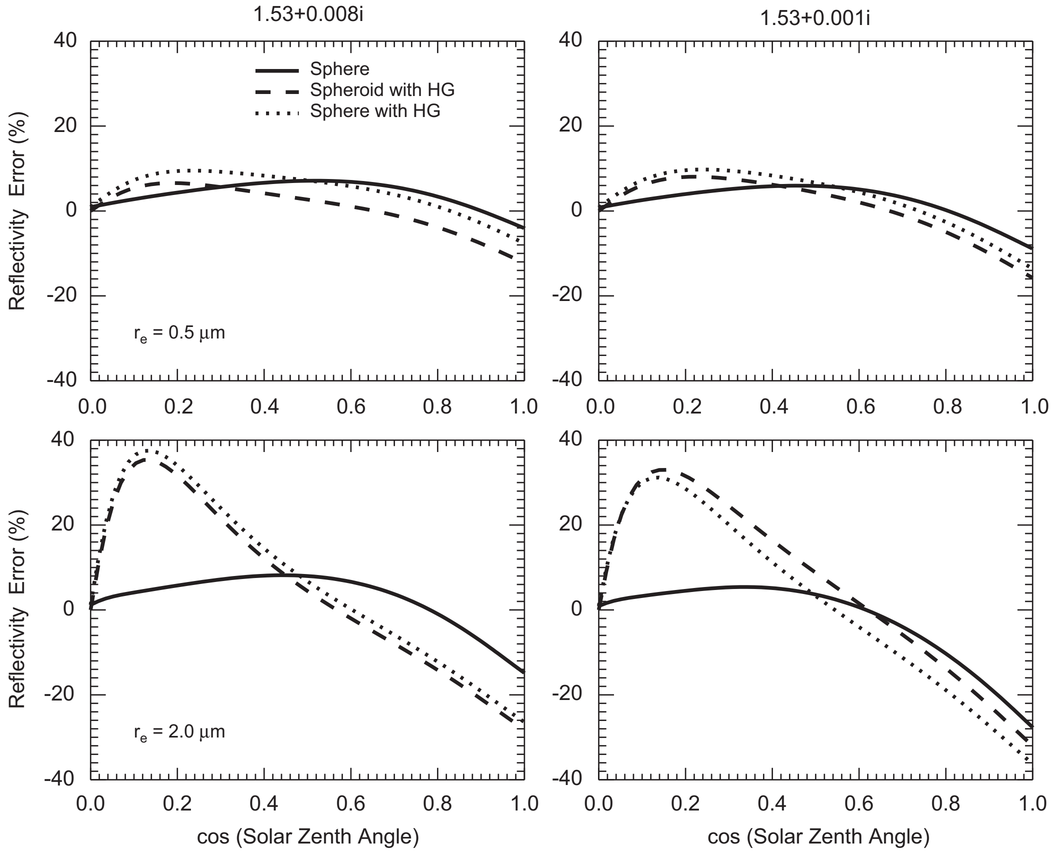

Fig. 3. Relative errors in reflectivity due to the use of the single-scattering properties (SSPs) along with the actual scattering phase function for spheres (solid line), SSPs along with the Henyey–Greenstein (HG) function for spheroids (dashed line) and spheres (dotted line) in the single-scattering limit (see Eq. (3.7)). The reference calculations are based on the SSPs along with the actual scattering phase function for spheroids. The results are shown for the refractive indices of 1.53+0.008i (left panel) and 1.53+0.001i (right panel) and the effective radii of 0.5 μm (upper panel) and 2 μm (lower panel) at the wavelength of 0.55 μm.

to approximate the spheroids are 0.3–0.8% in Q_e, 0.0–0.7% in $\tilde{\omega}$, and −1.6% to 2.3% in g. We also repeated the calculations in Table 1 using both *V*- and *P*-equivalent spheres, which shows larger errors.

Fig. 1 compares the scattering phase functions of spheroids and *V*/*P*-equivalent spheres for two refractive indices and two effective radii. The HG functions using the asymmetry factor of spheroids are also shown. The difference among the scattering phase functions increases as the r_e increases but this difference is less sensitive to m_i. It is also noted that for the scattering angle range from 0° to 90°, the phase function of spheres agrees with spheroids better than the HG function. The spherical scattering phase function is smaller than spheroids from ~90° to 145° but larger from ~145° to 180° while the HG function is systematically smaller from ~90° to 180°.

In this study, the number of the streams used in DISORT is determined by comparing the Legendre polynomial expansion of the scattering phase functions with their exact forms. As shown in Fig. 2, the expansion with 256 terms converges to the exact scattering phase functions for both spheroids and spheres (far fewer terms are needed to converge the HG function). Thus DISORT with 256-streams is used in our calculations.

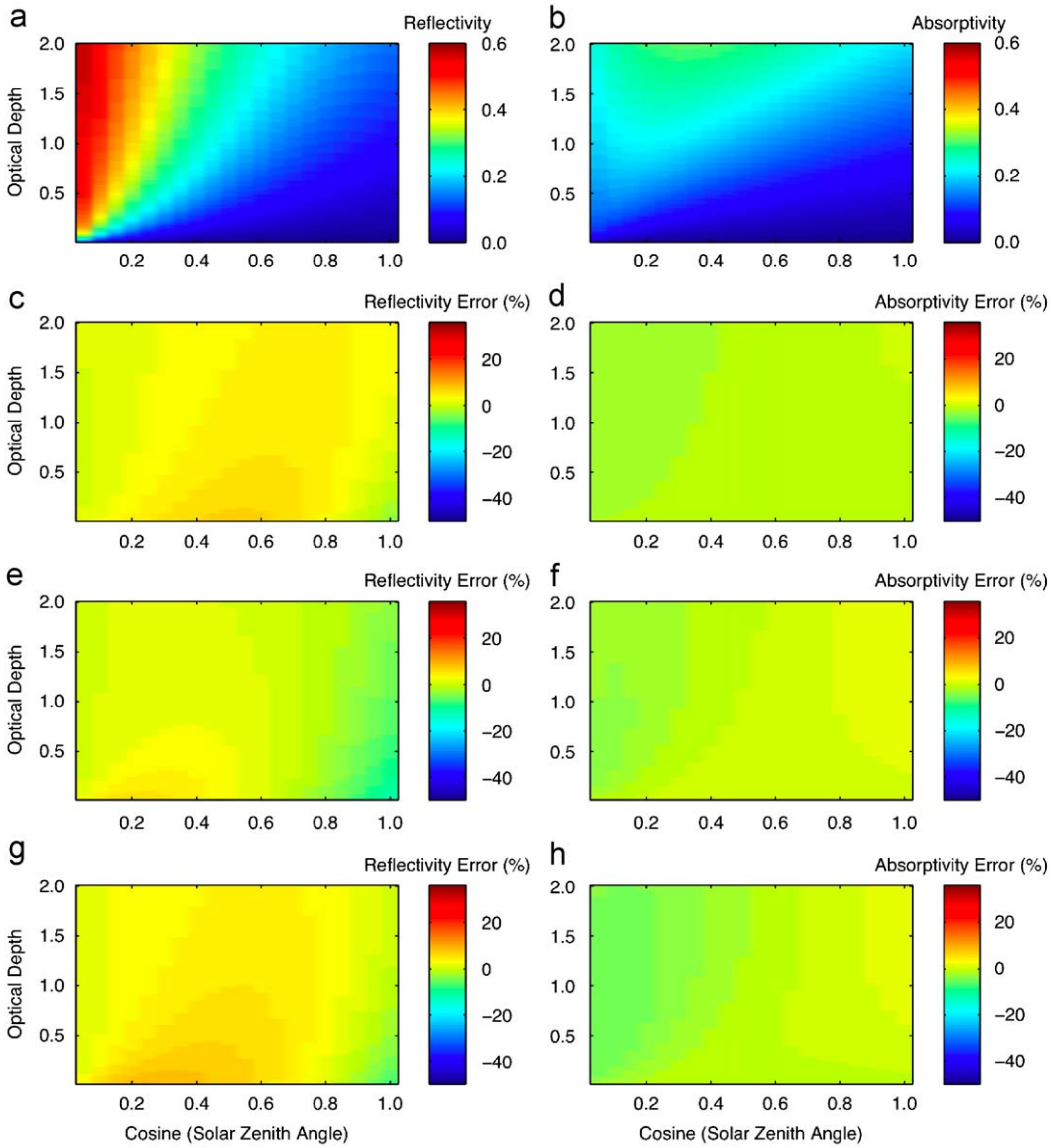

Fig. 4. (a) and (b) Reflectivity and absorptivity from the reference calculations; (c) an (d) relative errors in reflectivity and absorptivity due to the use of the single-scattering properties (SSPs) with the actual scattering phase function for spheres; (e) and (f) relative errors due to the use of SSPs with the Henyey–Greenstein (HG) function for spheroids; and (g) and (h) relative errors due to the use of SSPs with the HG function for spheres. An effective radius of 0.5 μm is considered along with refractive index of 1.53+0.008*i* at the wavelength of 0.55 μm. The delta-DISORT-256 stream is used in all calculations.

4.2. Errors in reflectivity under single-scattering limit

Fig. 3 shows the relative errors in reflectivity in the single-scattering limit (see Eq. (3.7)) due to the use of the SSPs along with the actual scattering phase function for spheres (solid line), SSPs along with the HG function for spheroids (dashed line) and spheres (dotted line). The reference calculations are based on the SSPs along with the actual scattering phase function for spheroids. For a given optical depth τ in the reference calculation, the approximate optical depth $\tau_{app} = \tau * Q_{e,app}/Q_{e,ref}$ where $Q_{e,app}$ and $Q_{e,ref}$ are extinction efficiencies of spheres and spheroids, respectively. Since the reflectivity is proportional to the optical depth and single-scattering albedo (see Eq. (3.7)), the relative errors associated with the extinction efficiency and single-scattering albedo are less than 1%. Thus the relative errors shown in Fig. 3 are largely caused by the differences in scattering phase functions.

Fig. 3 indicates that the relative errors increase as r_e increases but that the errors are not sensitive to the m_i. This result is consistent with the differences in scattering phase functions shown in Fig. 1. For a r_e of 2.0 μm, the larger errors associated with the HG function at $\mu_0 <\sim 0.5$ are due to the significant overestimation of the scattering phase function by the HG function near the scattering angle of $\sim 30^\circ$ (see Fig. 1). Smaller errors related to the use of the actual scattering phase function of spheres for larger μ_0 ($>\sim 0.7$) are because the errors in this phase function in the scattering angle range of 90–180° partly cancel each other (see Fig. 1). We can thus conclude from Fig. 3 that the use of actual scattering phase

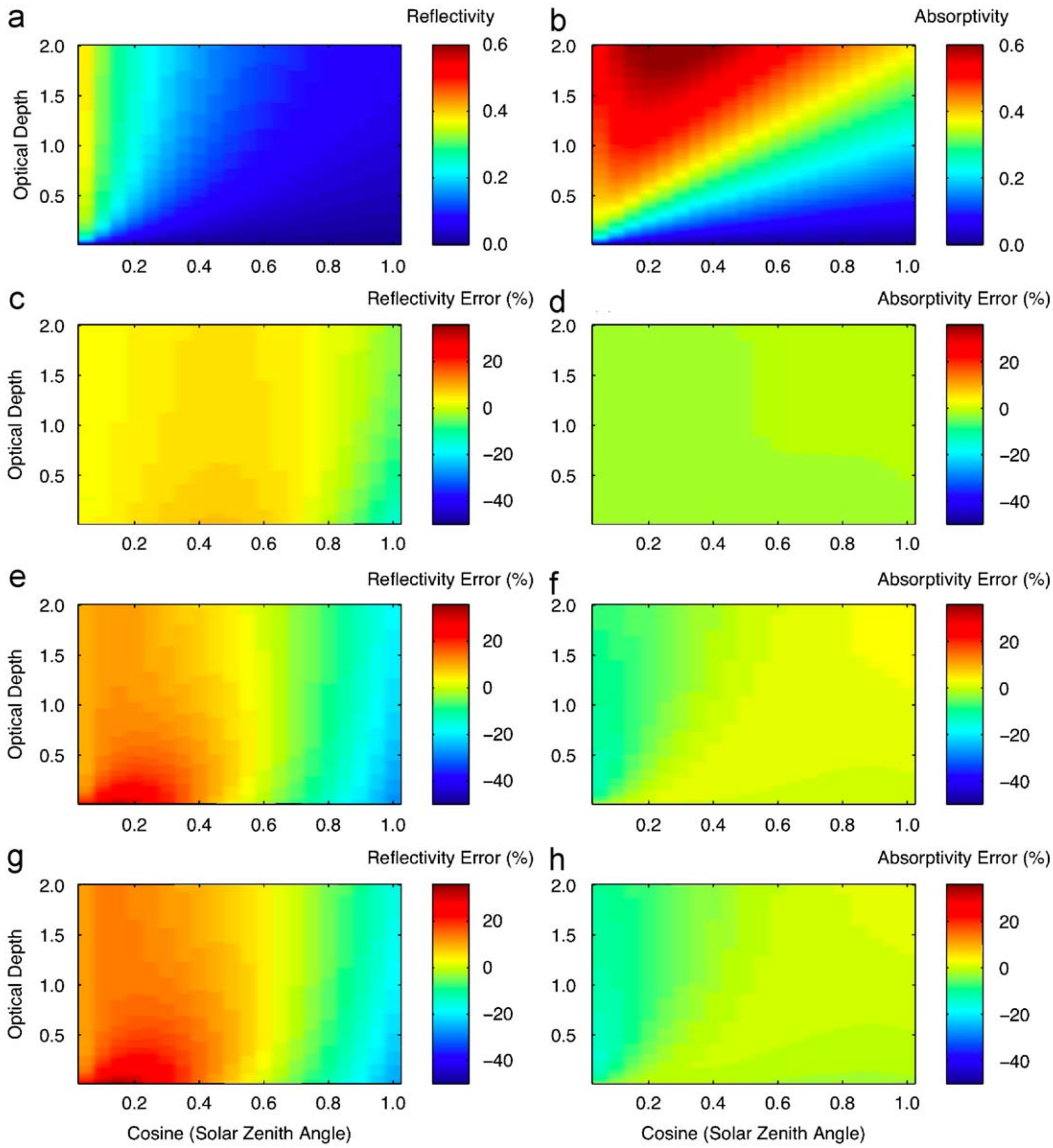

Fig. 5. Same as Fig. 4 except for an effective radius of 2.0 μm.

function of spheres generally introduces smaller errors than the use of HG functions. It is also noted that the errors using the HG function with the asymmetry factor based on spheroids and spheres are similar.

4.3. Errors in reflectivity and absorptivity of dust layers

Figs. 4(a) and (b) show the reference reflectivity and absorptivity versus the optical depth and cosine of solar zenith angle where the SSPs with the actual scattering phase function for spheroids are used. An effective radius of 0.5 μm is used along with refractive index of 1.53+0.008*i* at the wavelength of 0.55 μm. Figs. 4(c) and (d) show the corresponding relative errors due to the use of the SSPs with the actual scattering phase function for spheres; (e) and (f) show relative errors due to the use of SSPs with the HG function for spheroids; and (g) and (h) show relative errors due to the use of SSPs with the HG function for spheres. The delta-DISORT-256-steam is used in all above calculations. Fig. 5 is the same as Fig. 4 except for an effective radius of 2.0 μm.

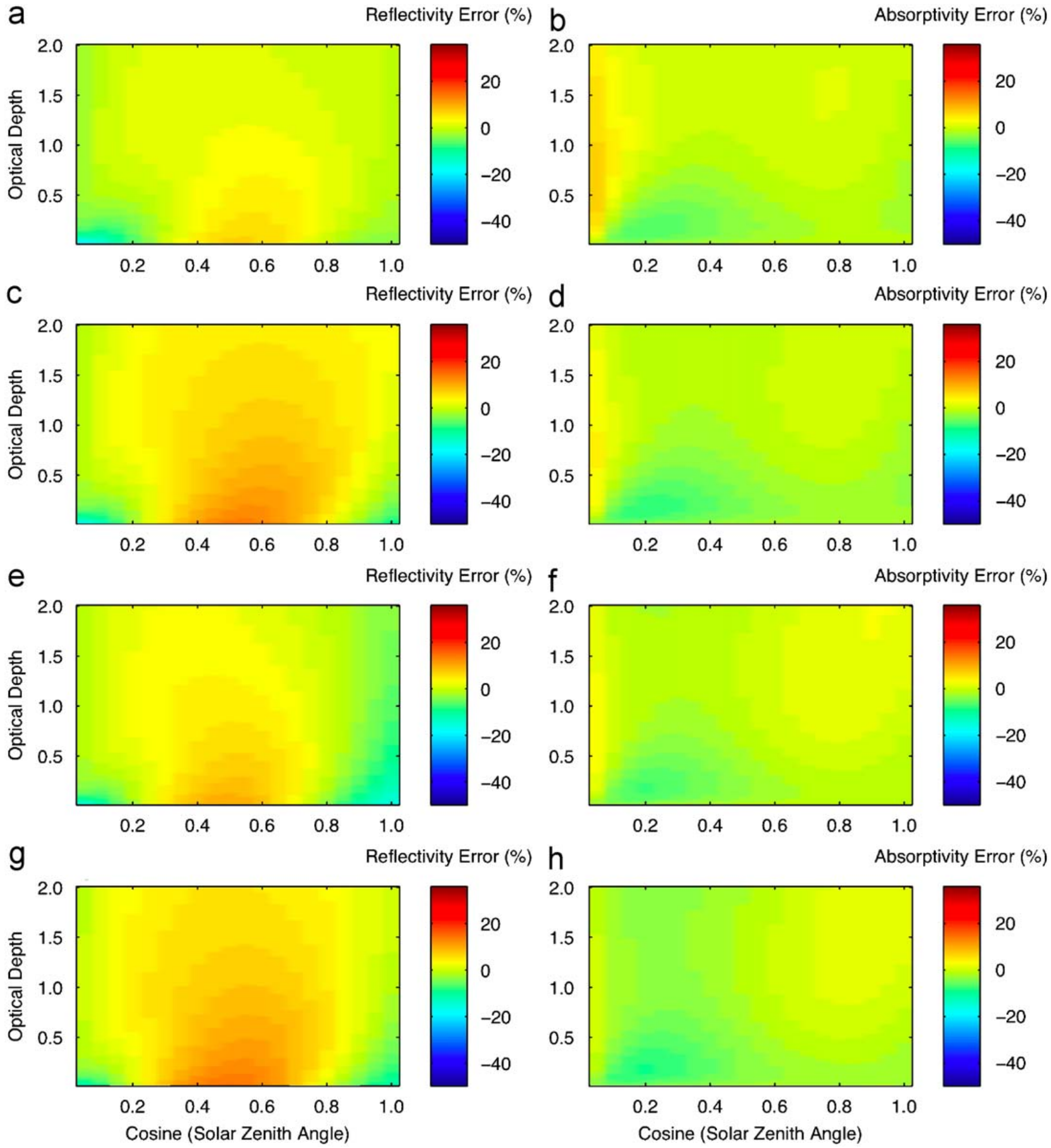

Fig. 6. Relative errors in reflectivity and absorptivity due to the delta-four-stream scheme using various single-scattering properties (SSPs) for dust aerosols: (a) and (b) the use of SSPs with $\tilde{\omega}_{1,2,3,4}$ from the actual scattering phase function for spheroids; (c) an (d) the use of the SSPs with $\tilde{\omega}_{1,2,3,4}$ from the actual scattering phase function for spheres; (e) and (f) the use of SSPs with $\tilde{\omega}_{1,2,3,4}$ from the Henyey–Greenstein (HG) function for spheroids; and (g) and (h) the use of SSPs with $\tilde{\omega}_{1,2,3,4}$ from the HG function for spheres. An effective radius of 0.5 μm is used along with refractive index of 1.53+0.008*i* at the wavelength of 0.55 μm.

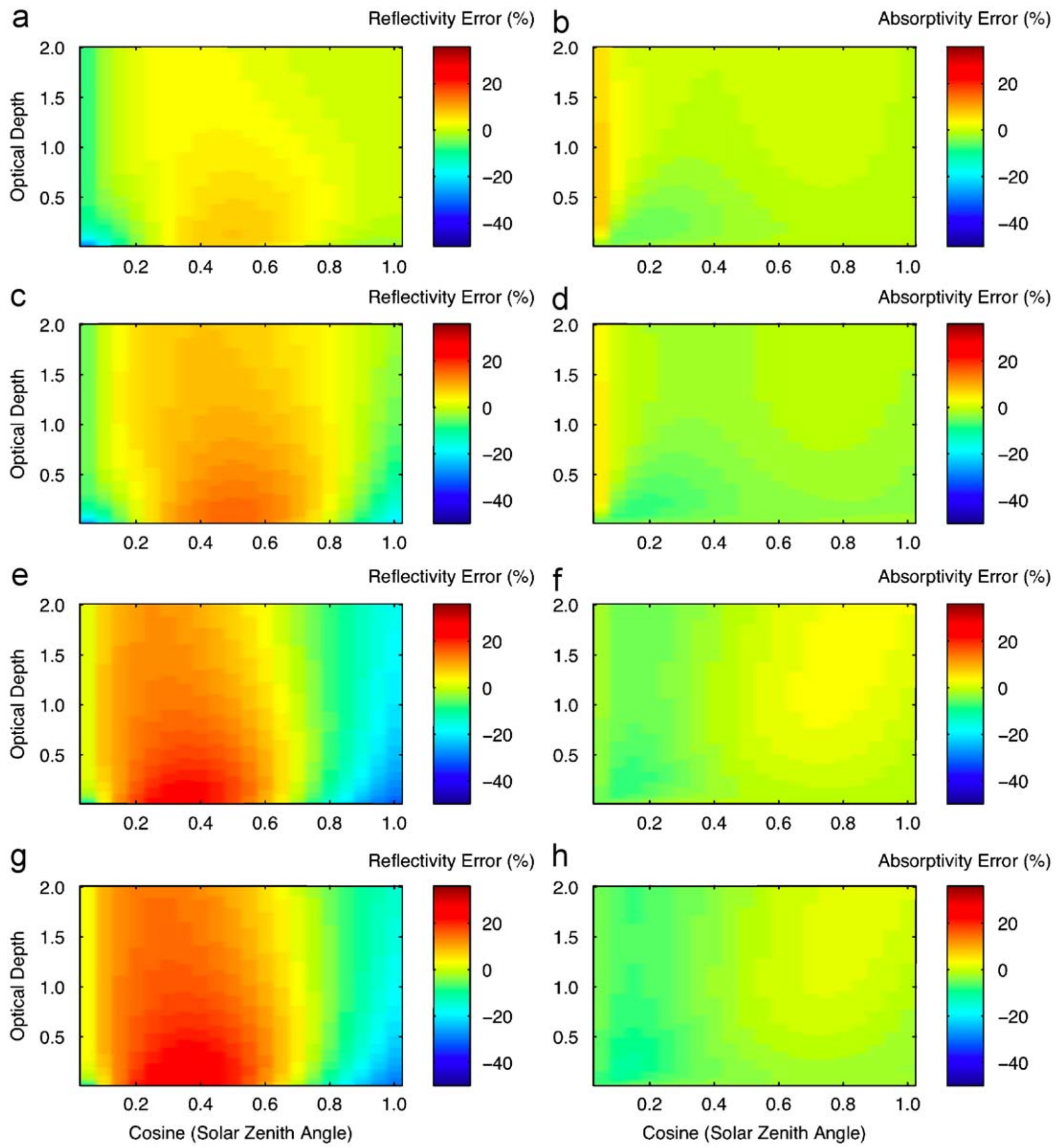

Fig. 7. Same as Fig. 6 except for an effective radius of 2.0 μm.

The dependences of relative errors on μ_0 in Figs. 4 and 5 when τ is small are very similar to those shown in Fig. 3 for the reflectivity. The relative errors in reflectivity become smaller as τ increases while the relative errors in absorptivity are small in all cases. The errors in reflectivity for a r_e of 2.0 μm are significantly larger than those for a r_e of 0.5 μm. In Fig. 5, the errors in (c) are smaller than (e) and (g) while the errors in (e) and (g) are similar. Thus we can conclude that the reflectivity errors in Fig. 5 are mainly associated with the use of the HG function instead of the SSPs for spheres. The reflectivity errors associated with various approximations shown in Fig. 4 ($r_e = 0.5$ μm) are similar, which are all generally small.

Fig. 6 shows relative errors in reflectivity and absorptivity due to the delta-four-stream scheme using various approximate SSPs for dust aerosol layers with an effective radius of 0.5 μm. The errors using SSPs with $\tilde{\omega}_{1,2,3,4}$ from the actual phase function for spheroids are shown in (a) and (b), using SSPs with $\tilde{\omega}_{1,2,3,4}$ from the actual phase function for spheres in (c) and (d), using spheroid SSPs with $\tilde{\omega}_{1,2,3,4}$ from the HG function in (e) and (f), and using sphere SSPs with $\tilde{\omega}_{1,2,3,4}$ from the HG function in (g) and (h). Fig. 7 is the same as Fig. 6 except for an effective radius of 2.0 μm.

The relative errors in absorptivity are small in all cases while the errors in reflectivity when $r_e = 2.0$ μm are significantly larger than those when $r_e = 0.5$ μm. In Fig. 7 (i.e., $r_e = 2.0$ μm), the reflectivity errors in (e) and (g) are similar while the errors in (a) are much smaller. Thus, in the delta-four-stream calculations, the reflectivity errors are still dominated by the

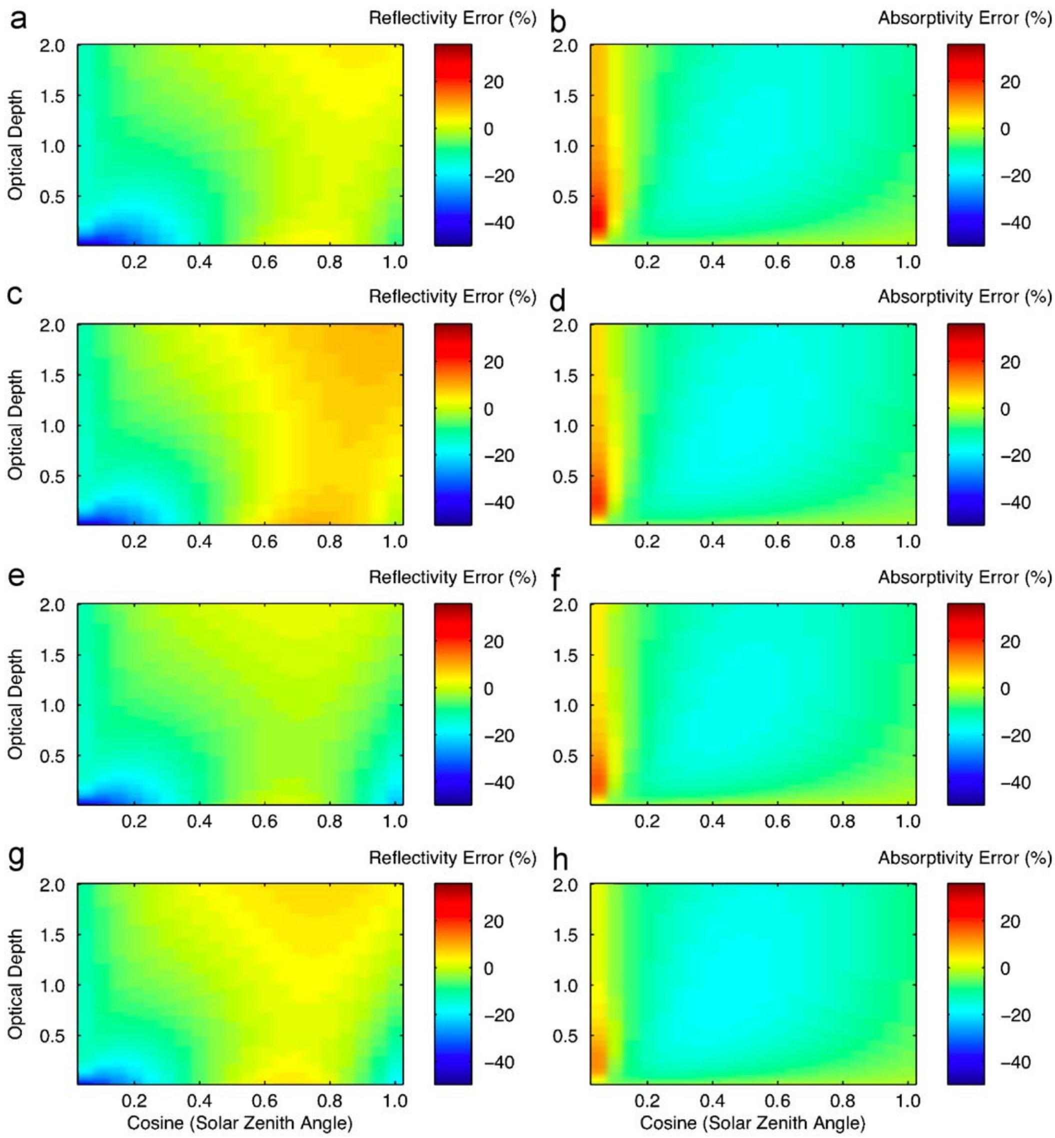

Fig. 8. Same as Fig. 6 except for the delta-two-stream scheme.

use of the HG function and the use of $\tilde{\omega}_{1,2,3,4}$ based on the actual phase function of spheroids may improve the accuracy of the simulated reflectivity.

Figs. 8 and 9 are the same as Figs. 6 and 7 except for the delta-two-stream scheme. The relative errors in both reflectivity and absorptivity using various approximate SSPs are similar, indicating that the errors associated with the radiative transfer scheme dominate. A close examination of Figs. 8 and 9 even suggests that the errors using $\tilde{\omega}_1$ and $\tilde{\omega}_2$ based on the HG functions are slightly smaller than those using $\tilde{\omega}_1$ and $\tilde{\omega}_2$ based on the actual phase functions (e and f versus a and b; g and h versus c and d). This might be because the errors due to the delta-two-stream scheme partly cancel the errors due to the HG functions.

Fig. 10 shows relative errors in global albedo versus optical depth for $r_e = 0.5\,\mu$m (left panel) and $2.0\,\mu$m (right panel). The errors using the delta-DISORT-256 stream, delta-four-stream, and delta-two-stream schemes are shown in the upper, middle, and lower panels, respectively. Solid lines represent SSPs with the actual scattering phase function for spheres, dashed lines show spheroid SSPs with HG function, dotted lines show sphere SSPs with HG function, and dashed-dotted lines indicate SSPs with the actual scattering phase function for spheroids (only in middle and lower panels). The errors in the upper panel are due to the approximate SSPs only, while errors in middle and lower panels are caused by both approximate SSPs and radiative transfer schemes.

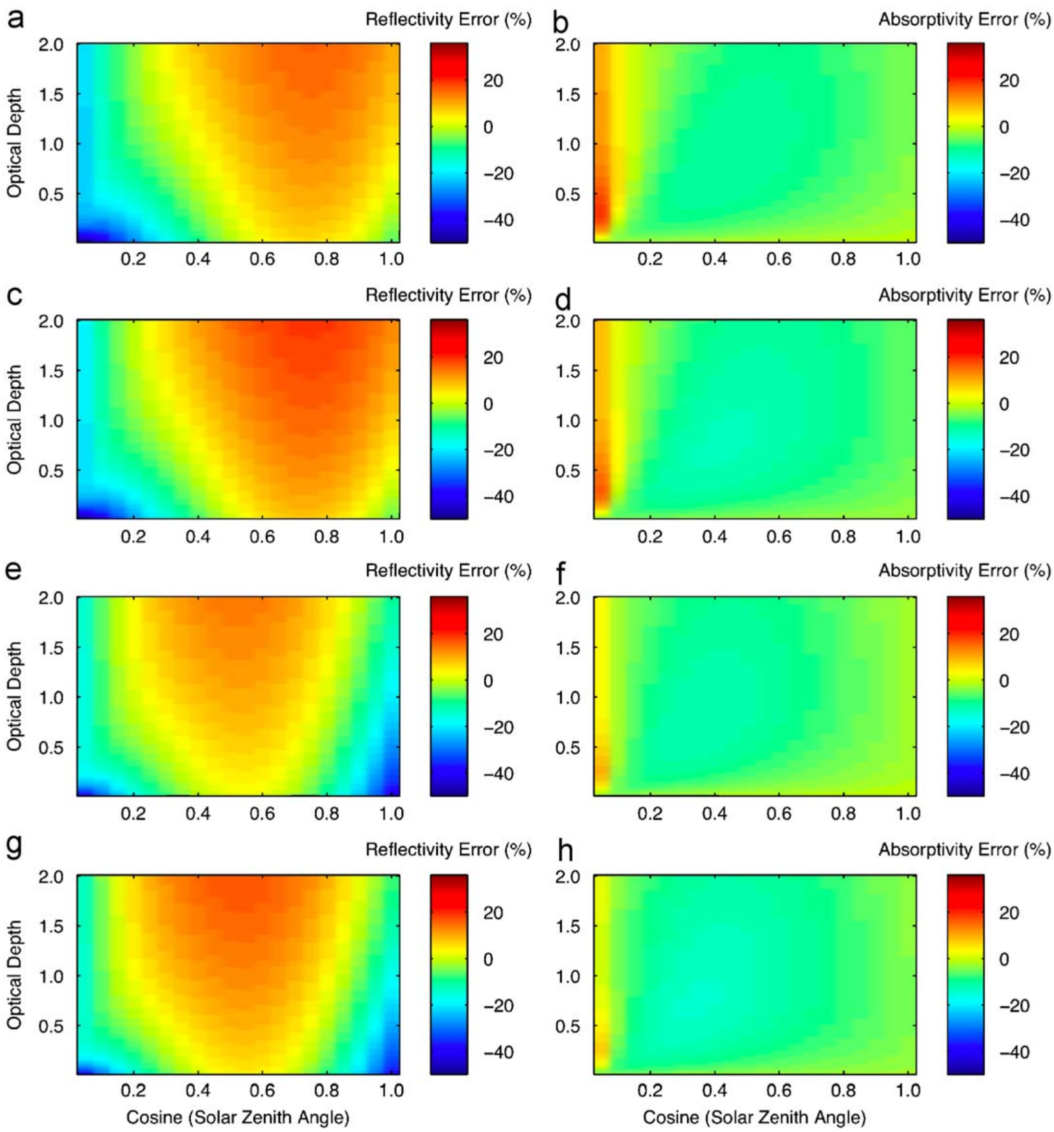

Fig. 9. Same as Fig. 7 except for the delta-two-stream scheme.

In the upper panel, the relative errors in global reflectivity due to the use of the SSPs with the actual phase function for spheres (solid lines) are less than 5%. In the middle and lower panels, the relative error difference between the solid and dashed-dotted lines is also less than 5%, as is the difference between dashed and dotted lines in all panels. Thus we can conclude that the relative error in the global reflectivity due to the use of sphere SSPs is always less than 5%.

We also examine the errors for the refractive index of 1.53+0.001*i*, which are similar to those shown in Figs. 4–10.

5. Summary and conclusions

The SSPs of dust aerosols with both spheroidal and *V*/*P*-equivalent-spherical shapes are simulated at the wavelength of 0.55 μm for two refractive indices and four effective radii. It is shown that the relative errors due to the use of the spheres to approximate the spheroids are less than 1% in extinction efficiency and single-scattering albedo, and less than 2% in asymmetry factor. By comparing the scattering phase functions of *V*/*P*-equivalent spheres and the HG function with those of spheroids, it is found that in the scattering angle range of 0–90°, the phase function of spheres agrees with spheroids better than the HG function. In the range of ~90–180°, the HG function is systematically smaller while the spherical scattering phase function is smaller from ~90° to 145° but larger from ~145° to 180°.

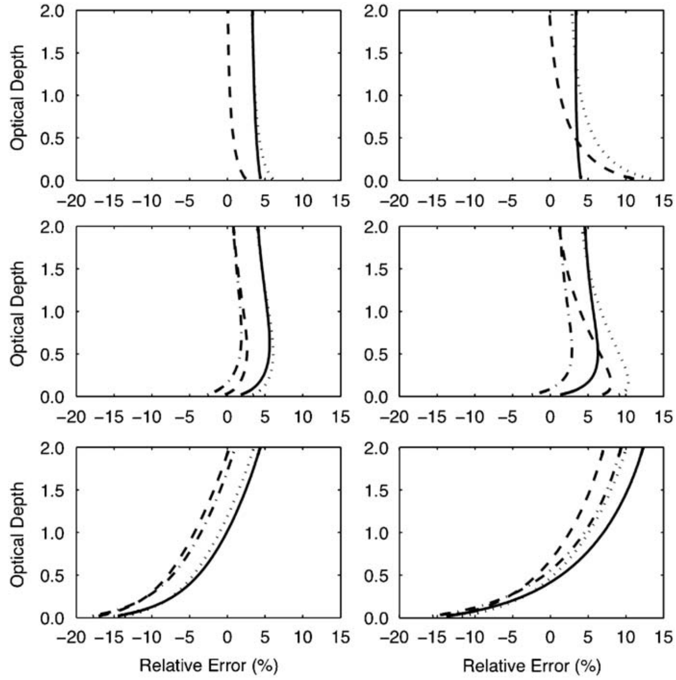

Fig. 10. Relative errors in global albedo versus optical depth for $r_e = 0.5\,\mu$m (left panel) and 2.0 μm (right panel) with refractive index of 1.53+0.008*i* at the wavelength of 0.55 μm. The results from delta-DISORT-256 stream, delta-four-stream, and delta-two-stream schemes are shown in the upper, middle, and lower panels, respectively. The solid line denotes the use of single-scattering properties (SSPs) and the actual phase function for spheres, dashed line the use of spheroid SSPs and Henyey–Greenstein (HG) function, dotted line the use of sphere SSPs and HG function, and dashed-dotted line the use of SSPs and the actual phase function for spheroids (only in middle and lower panels).

We examine the errors in reflectivity and absorptivity due to the use of SSPs of *V*/*P*-equivalent spheres and HG functions for dust aerosols. The reference calculation is based on the delta-DISORT-256-stream scheme using the SSPs of the spheroids. It is found that the errors are mainly caused by the use of the HG function instead of the SSPs of spheres. This result is validated by the solution under the single-scattering limit.

We also examine the errors associated with the delta-four- and delta-two-stream schemes using various approximate SSPs for dust aerosol layers. For the delta-four-stream scheme, the errors are found to be still dominated by the use of the HG function, and the use of $\tilde{\omega}_{1,2,3,4}$ from the actual scattering phase function of spheroids may help reduce the errors. For the delta-two-stream calculations, the errors associated with the radiative transfer scheme dominate. It is also shown that the relative errors in the global reflectivity due to the use of sphere SSPs are always less than 5%. We conclude that the Mie-based SSPs of spheroidal dust aerosols are well suited in radiative flux calculations.

Acknowledgments

This research is supported by NASA Grants NNX08AF66G and NNX08AG91G. It is also supported by National Science Foundation of China under Grants (40628005 and 40633017) and National Basic Research Program of China (2006CB400501). We thank Prof. P. Yang for providing geometric ray-tracing program and Mr. G. Hong for useful discussions.

References

[1] Zender CS. Quantifying mineral dust mass budgets: terminology, constraints, and current estimates. EOS 2004;85:509–12.
[2] Slingo A, et al. Observations of the impact of a major Saharan dust storm on the atmospheric radiation balance. Geophys Res Lett 2006;33:L24817.
[3] Huang JP, Fu Q, Su J, Tang Q, Minnis P, Hu YX, et al. Taklimakan dust aerosol radiative heating derived from CALIPSO observations using the Fu-Liou radiation model with CERES constraints. Atmos Chem Phys 2009, submitted for publication.
[4] Twomey S. The influence of pollution on the shortwave albedo of clouds. J Atmos Sci 1977;34:1149–52.
[5] Albrecht BA. Aerosols, cloud microphysics, and fractional cloudiness. Science 1989;245:1227–30.
[6] Mahowald N, Baker A, Bergametti G, Brooks N, Duce R, Jickells T, et al. Atmospheric global dust cycle and iron inputs to the ocean. Global Biogeochem Cycles 2005;19:4025.
[7] Forster P, et al. Changes in atmospheric constituents and in radiative forcing. In: Solomon S, et al., editors. Climate change 2007: the physical science basis. Contribution of Working Group I to the fourth assessment report of the intergovernmental panel on climate change. Cambridge: Cambridge University Press; 2007.

[8] Okada O, Heintzenberg J, Kai K, Qin Y. Shape of atmospheric mineral particles collected in three Chinese arid-regions. Geophys Res Lett 2001;28:3123–6.
[9] Munoz O, Volten H, de Haan JF, Vassen W, Hovenier JW. Experimental determination of scattering matrices of randomly oriented fly ash and clay particles at 442 and 633 nm. J Geophys Res Atmos 2001;106:22833–44.
[10] Kalashnikova OV, Sokolik IN. Modeling the radiative properties of nonspherical soil-derived mineral aerosols. J Quant Spectrosc Radiat Transfer 2004;87:137–66.
[11] Mishchenko MI, Travis LD, Kahn RA, West RA. Modeling phase functions for dustlike tropospheric aerosols using a shape mixture of randomly oriented polydisperse spheroids. J Geophys Res Atmos 1997;102:16831–47.
[12] Yang P, Feng Q, Hong G, Kattawar GW, Wiscombe WJ, Mishchenko MI, et al. Modeling of the scattering and radiative properties of nonspherical dustlike aerosols. J Aerosol Sci 2007;38:995–1014.
[13] Zhao XP, Laszlo I, Dubovik O, Holben BN, Sapper J, Tanre D, et al. A study of the effect of non-spherical dust particles on the AVHRR aerosol optical thickness retrievals. Geophys Res Lett 2003;30:1317.
[14] Wang J, Liu X, Christopher S, Reid J, Reid E, Maring H. The effects of non-sphericity on geostationary satellite retrievals of dust aerosols. Geophys Res Lett 2003;30:2293.
[15] Dubovik O, et al. Application of spheroid models to account for aerosol particle nonsphericity in remote sensing of desert dust. J Geophys Res 2006;111:D11208.
[16] d'Almeida GA, Koepke P, Shettle EP. Atmospheric aerosols: global climatology and radiative characteristics. A Deepak Publishing; 1991.
[17] Tegen I, Lacis AA. Modeling of particle size distribution and its influence on the radiative properties of mineral dust aerosol. J Geophys Res 1996;19:237–44.
[18] Levoni C, Cervino M, Guzzi R, Torricella F. Atmospheric aerosol optical properties: a database of radiative characteristics for different components and classes. Appl Opt 1997;36:8031–41.
[19] Collins WD, Rasch PJ, Eaton BE, Fillmore DW, Kiehl JT, Beck CT, et al. Simulation of aerosol distributions and radiative forcing for INDOEX: regional climate impacts. J Geophys Res 2002;107(D19):8028.
[20] Grenfell TC, Warren SG. Representation of a nonspherical ice particle by a collection of independent spheres for scattering and absorption of radiation. J Geophys Res 1999;104:31697–709.
[21] Pollack JB, Cuzzi JN. Scattering by non-spherical particles of size comparable to a wavelength: a new semi-empirical theory and its application to tropospheric aerosols. J Atmos Sci 1980;37:868–81.
[22] Foot JS. Some observations of the optical properties of clouds, II, Cirrus. Quart J R Meteorol Soc 1988;114:145–64.
[23] Fu Q. An accurate parameterization of the solar radiative properties of cirrus clouds for climate models. J Climate 1996;9:2058–82.
[24] Nakajima T, Tanaka M, Yamano M, Shiobara M, Arao K, Nakanishi Y. Aerosol optical characteristics in the yellow sand events observed in May, 1982 at Nagasaki—part II. Models. J Meteorol Soc Jpn 1989;67:279–91.
[25] Dubovik O, Holben BN, Eck TF, Smirnov A, Kaufman YJ, King MD, et al. Variability of absorption and optical properties of key aerosol types observed in worldwide locations. J Atmos Sci 2002;59:590–608.
[26] Mishchenko MI, Travis LD, Lacis AA. Scattering, absorption, and emission of light by small particles. Cambridge: Cambridge University Press; 2002.
[27] Yang P, Liou KN. Geometric-optics-integral-equation method for light scattering by nonspherical ice crystals. Appl Opt 1996;35:6568–84.
[28] Vouk V. Projected area of convex bodies. Nature 1948;162:330–1.
[29] Bryant FD, Latimer P. Optical efficiencies of large particles of arbitrary shape and orientation. J Colloid Interface Sci 1969;30:291–304.
[30] Mitchell DL, Arnott WP. A model predicting the evolution of ice particle size spectra and radiative properties of cirrus clouds. Part II: dependence of absorption and extinction on ice crystal morphology. J Atmos Sci 1994;51:817–32.
[31] Fu Q, Yang P, Sun WB. An accurate parameterization of the infrared radiative properties of cirrus clouds for climate models. J Climate 1998;11:2223–37.
[32] Fu Q, Sun WB, Yang P. On modeling of scattering and absorption by nonspherical cirrus ice particles in thermal infrared wavelengths. J Atmos Sci 1999;56:2937–47.
[33] Nakajima T, Glauco T, Rao R, Boi P, Kaufman Y, Holben B. Use of sky brightness measurements from ground for remote sensing of particulate polydispersions. Appl Opt 1996;35:2672–86.
[34] Diner DJ, Paradise SR, Martonchik JV. Development of an aerosol opacity retrieval algorithm for use with multi-angle land surface images. In: Proceedings of the IGARSS'94, vol. 3, Pasadena, CA, 1994. p. 1664–6.
[35] Hansen JE, Travis LD. Light scattering in planetary atmospheres. Space Sci Rev 1974;16:527–610.
[36] Stamnes K, Tsay S, Wiscombe W, Jayaweera K. Numerically stable algorithm for discrete-ordinate-method radiative transfer in multiple scattering and emitting layered media. Appl Opt 1988;27:2502–9.
[37] Wiscombe W. The delta-M method: rapid yet accurate radiative flux calculations for strongly asymmetric phase functions. J Atmos Sci 1977;34:1408–22.
[38] Liou KN, Fu Q, Ackerman TP. A simple formulation of the delta-four-stream approximation for radiative transfer parameterization. J Atmos Sci 1988;45:1940–7.
[39] Liou KN. An introduction to atmospheric radiation. New York: Academic Press; 2002 [second version].